PAPER

Check for updates

Diffusion doping of cobalt in rod-shape anatase TiO₂ nanocrystals leads to antiferromagnetism†

Shahzahan Mia, [a] Shelton J. P. Varapragasam, [a] Aravind Baride, [a]
Choumini Balasanthiran, [b] Balamurugan Balasubramanian, [d]
Robert M. Rioux [bc] and James D. Hoefelmeyer *[a]

Cobalt(II) ions were adsorbed to the surface of rod-shape anatase TiO₂ nanocrystals and subsequently heated to promote ion diffusion into the nanocrystal. After removal of any remaining surface bound cobalt, a sample consisting of strictly cobalt-doped TiO₂ was obtained and characterized with powder X-ray diffraction, transmission electron microscopy, UV-visible spectroscopy, fluorescence spectroscopy, X-ray photoelectron spectroscopy, SQUID magnetometry, and inductively-coupled plasma atomic emission spectroscopy. The nanocrystal morphology was unchanged in the process and no new crystal phases were detected. The concentration of cobalt in the doped samples linearly correlates with the initial loading of cobalt(II) ions on the nanocrystal surface. Thin films of the cobalt doped TiO₂ nanocrystals were prepared on indium-tin oxide coated glass substrate, and the electrical conductivity increased with the concentration of doped cobalt. Magnetic measurements of the cobalt-doped TiO₂ nanocrystals reveal paramagnetic behavior at room temperature, and antiferromagnetic interactions between Co ions at low temperatures. Antiferromagnetism is atypical for cobalt-doped TiO₂ nanocrystals, and is proposed to arise from interstitial doping that may be favored by the diffusional doping mechanism.

Introduction

The properties of nanocrystals can be selected based on tuning crystal size,[1–3] crystal shape,[4–8] and the surface termination.[9,10] In addition, the composition of a crystal can be adjusted to yield solid solutions. A widely explored example is the doping of semiconductor nanocrystals, in which control of the impurity concentration may be correlated with optoelectronic, magnetic, or other properties.[11] However, the precise control of the composition of doped nanocrystals remains a significant challenge.[12,13] In the most extreme case, the atom-precise number and location of impurity atoms can afford nanocrystals with distinct properties. CdSe nanocrystals lightly doped with Ag revealed unexpected complexity, and exhibited a large enhancement of fluorescence at low doping.[14] Recently developed 'solotronic' nanocrystals, in which a single impurity or

defect is present in a semiconductor nanocrystal, exhibit remarkable properties.[15–17] Optical or electrical stimulus of quantum dots with single atom manganese impurity led to specific changes in the manganese spin state,[18,19] and gave rise to well-resolved splitting of the photoluminescence due to the spin projections of the $S = 5/2$ Mn²⁺ ion.[20] Despite significant advances in the synthesis of doped nanocrystals, the ability to selectively locate impurities at specific sites (substitutional *vs.* interstitial), control the concentration and spatial density of the impurity in the host, and control the charge compensation mechanism remain as open challenges in the preparation of doped nanocrystals.[21]

Examples of doped nanocrystal materials are abundant in the literature; however, a common and important oversight concerns the speciation of the impurity atom within the nanocrystal and the surface. If one is to prepare a doped nanocrystal sample and assign specific properties that arise from the presence of the dopant, then it is critically important to develop protocols for the selective removal of impurities adsorbed on the surface of nanocrystals after the doping procedure, as the adsorbed impurities contribute markedly different properties than the doped impurities.[11,22,23] Without a standardization of practice to remove surface adsorbed 'dopant' from samples of doped nanocrystals, there may be confusion as to the properties that arise from dopant ions *versus* those that arise from adsorbate surface ions. One method to resolve this issue is to utilize

aDepartment of Chemistry, University of South Dakota, 414 E. Clark St., Vermillion, SD 57069, USA. E-mail: james.hoefelmeyer@usd.edu

bDepartment of Chemical Engineering, The Pennsylvania State University, 22 Chemical Biomedical Engineering Building, University Park, Pennsylvania, 16802-4400, USA

cDepartment of Chemistry, The Pennsylvania State University, 22 Chemical Biomedical Engineering Building, University Park, Pennsylvania, 16802-4400, USA

dNebraska Center for Materials and Nanoscience, Department of Physics and Astronomy, University of Nebraska, Lincoln, NE 68588-0299, USA

† Electronic supplementary information (ESI) available. See DOI: 10.1039/d0na00640h

a trapped dopant model in which surface impurities become entombed upon growing an overlayer of host material.[24,25] Another method is to remove surface adsorbates after the preparation of doped nanocrystals. For example, trioctylphosphine oxide was used to remove surface Co^{2+} ions from cobalt doped TiO_2 nanocrystals.[26]

A number of synthetic routes have been devised to incorporate dopants into nanocrystals, including single source precursors, growth-doping, nucleation-doping, and cation diffusion.[27,28] In the cation diffusion method, the dopant is introduced by diffusion into nanocrystals. This method has several advantages. Well-defined nanocrystals can be prepared in the absence of dopant without the complications of additional reactants in the parent nanocrystal synthesis, thereby allowing control of nanocrystal morphology. Ion diffusion in nanocrystals can be fast compared to bulk materials. There is potential to control the dopant concentration in the nanocrystal host by adjusting reaction conditions such as temperature and dopant ion concentration in solution. Despite its potential as a synthetic route for the preparation of doped nanocrystals, the use of cation diffusion for their preparation is rather limited.[2,29–33]

We demonstrate an ion-diffusion route that leads to doping of cobalt into anatase TiO_2 nanocrystals. The principle is based on the controlled adsorption of cobalt ions onto the surface of the nanocrystal[34] followed by ion diffusion at elevated temperature. We show a linear correlation between the loading of cobalt ion on the nanocrystal surface in the reactant and cobalt dopant in the nanocrystal product. This feature of the synthesis allows for the rational design of cobalt doped anatase TiO_2 nanocrystals with precise selection of the dopant concentration. Electrical conductivity measurements of thin-film cobalt doped anatase TiO_2 nanocrystals were obtained, and conductivity increased with increasing cobalt concentration. The cobalt doped anatase TiO_2 nanocrystals exhibit room temperature paramagnetism and at low temperatures there is antiferromagnetic ordering.

Experimental

Chemicals

Titanium(IV) tetraisopropoxide (98+%, Acros Organics), oleic acid (97%, Fisher Scientific), cobalt(II) chloride hexahydrate (TCI), oleylamine (TCI), 1-octadecene (90% technical grade, Acros), trioctylphosphine oxide (Eastman Organic Chemicals), dimethylglyoxime (Mallinckrodt Chemical), indium tin oxide coated glass (Delta Technologies), were used as received. Solvents (ethanol, isopropanol, tetrahydrofuran, hexanes) were purchased from Fisher Scientific and used without purification. Rod-shape anatase TiO_2 nanocrystals[35] (hereafter denoted as 'TiO₂ nanorods') and $Co^{2+}_{(surface)}$–TiO_2 nanorods[34] were prepared as reported in the literature.

Synthesis of Co$_{(doped)}$–TiO₂ nanorods

Briefly, 8 mL of 1-octadecene and $Co^{2+}_{(surface)}$–TiO_2 nanorods (4 mmol) were added to a 100 mL three-neck roundbottom flask.

Volatiles were evacuated at 120 °C for 1 h. After cooling under N_2 flow, a solution of trioctylphosphine oxide (1 g, 2.6 mmol) in 12 mL of 1-octadecene was added to the flask. Under N_2 flow, the mixture was heated to 250 °C for 14 h. The reaction was quenched with 5 mL of toluene. The product was precipitated using isopropanol. The precipitate was separated by centrifugation at 3500 rpm for 8 min, followed by redispersion in hexanes. The precipitation and redispersion process was carried out for four cycles to remove solution phase cobalt ion or ligands from the product. The final dispersion was centrifuged at 3500 rpm for 8 min to remove any insoluble particles. Note: the material at this stage has surface cobalt ions and doped cobalt ions. Removal of surface Co(II) ions: a centrifuge tube was charged with 0.5 mmol of cobalt doped TiO_2 nanorods in 5 mL tetrahydrofuran. To this, dimethylglyoxime was added to supply a 10 : 1 ratio of dimethylglyoxime : cobalt. The contents were sonicated at room temperature for 10 min and the color changed to brown. The products were centrifuged at 10 500 rpm for 5 min to yield a sticky dark brown precipitate and brown supernatant. The supernatant was kept, and ethanol was added to induce flocculation. The mixture was centrifuged at 2200 rpm for 3 min. A tan precipitate and brown supernatant were observed. The precipitate was identified as cobalt doped TiO_2 NRs. Redispersion of the tan precipitate gave a cloudy suspension that became transparent upon addition of 1 drop of oleylamine. The sample was precipitated/re-dispersed four times from ethanol/hexanes and used for characterization.

Thin film preparation and conductivity measurements

TiO_2 nanorod or cobalt-doped TiO_2 nanorod thin films were prepared on ITO coated glass substrates (1 in²; 16 Ω). In our process, a single layer of nanorods was applied by dropcasting 200 μL of 0.12 mM nanorods dispersed in hexanes from a micropipette over the course of 30 seconds onto the spinning substrate (3000 rpm). The spin rate was controlled with a spin-coater (Laurell Technologies, Corp. WS-400B-6NPP/LITE). Following each spincoated nanorod layer, the films were calcined at 450 °C in air for 1 h (heating rate = 9 °C min^{-1}). Additional layers could be applied by repeating the spincoat and calcination steps. The resistance of each film was found from four-point probe measurements using a Signatone S-301-4 probe.

Characterization

Transmission electron microscopy (TEM) images were obtained using a Tecnai Spirit G² Twin TEM instrument with a LaB₆ filament operating at 120 kV. Samples were dropcast onto carbon thin film supported on 200 mesh copper grids (Electron Microscopy Sciences). Digital images were obtained by projection onto Gatan US1000 or SC200 CCD Digital Camera and recorded with Digital Micrograph software. Powder X-ray diffraction (XRD) patterns were collected using a Rigaku Ultima IV in focused beam Bragg–Brentano geometry with 5° soller slits and 2/3-degree scatter slits in the incident and exit beams, 10 mm divergence height limiting slit in the incident beam, and 0.45 mm receiving slit. The diffraction patterns were

recorded at room temperature employing Ni-filtered Cu Kα radiation ($\lambda = 1.5408$ Å), using an accelerating voltage of 40 kV, and emission current of 44 mA. Data was collected from 10–80 (2-theta) with the step size of 0.02°. Analysis of the XRD data was conducted using whole pattern powder fitting feature of the Rigaku PDXL software. Crystallite size was calculated using Williamson – Hall Method and Lattice parameter were calculated using whole pattern powder fitting (WPPF) method. UV-visible spectra were obtained from a Varian Cary 50 spectrophotometer. Photoluminescence spectra were acquired on a Fluoromax-4 fluorometer (JY Horiba) using 90° collection geometry. The samples were dispersed in hexanes and placed in 1 cm pathlength quartz cuvettes. Elemental analyses were obtained using an Agilent Technologies 700 Series inductively coupled plasma optical emission spectroscopy (ICP-OES) instrument. A 20–40 mg portion of sample was digested with *aqua regia*, then heated at 150–200 °C to evaporate the acids. The remaining solids were dissolved in 10% HNO_3 and filtered to remove the insoluble TiO_2. Scanning electron micrographs (SEM images) were acquired using a field emission SEM (Zeiss SIGMA, 30 kV) mounted with a Schottky field emission filament. The thin-film samples were directly used without any conductive coating. To obtain the transverse sectional view of the film coating, a fault line was applied using a diamond cutter on the backside of the thin-film coated ITO glass and the ITO glass was fractured along the fault line into two halves. One half was mounted vertically onto the SEM stage for imaging. An Everhart-Thornley detector was used to capture secondary electron signal. Micrographs were analyzed using the ImageJ software. Quantum Design MPMS superconducting quantum interference device (SQUID) was used to measure the magnetic properties. X-ray photoelectron spectroscopy (XPS) measurements were carried out using monochromatic Al K_a X-ray with an energy of 1486.6 eV by Thermo Scientific K-alpha$^+$ XPS.

Results

We prepared anatase TiO_2 nanorods according to the procedure reported by Hyeon.[35] The reaction yields multigram quantities of nanocrystals. The anatase phase was confirmed based on the powder X-ray diffraction data from the sample (Fig. 1). Anisotropy of the nanocrystals is evident based on the markedly narrower linewidth of the (004) reflection that is consistent with

nanocrystals elongated along the c axis. The rod shape morphology was immediately evident from TEM data from the sample (Fig. 1). The average diameter was 3.2 ± 0.5 nm and average length was 42.9 ± 7.7 nm. The (101) and (004) lattice fringes were observed with interplanar spacings well-matched to the d-spacings derived from X-ray diffraction data and consistent with the known structure of anatase TiO_2. The (004) lattice fringes are perpendicular to the longitudinal axis of the nanocrystal and confirm the elongation of the crystal along the c axis. The nanocrystals are passivated with oleic acid and disperse in non-polar solvents. A UV-visible spectrum was recorded from the diluted dispersion of TiO_2 nanorods in hexanes (Fig. 1). An intense ligand to metal charge transfer (LMCT) feature was observed with two maxima at 240 and 286 nm. The absorbance feature is strongly blue-shifted in comparison with bulk anatase TiO_2, consistent with quantum confinement of the exciton due to the small diameter of the nanocrystal.

In previous work, we established a robust protocol for the adsorption of metal ions onto the surface of TiO_2 nanorods as a synthesis method.[34,36,37] The reaction is self-limiting based on the number of surface titanium atoms on the nanocrystal. In the example of Co^{2+} adsorbed onto the surface of TiO_2 we observe nearly quantitative uptake of Co^{2+} for Co : Ti mass ratio below ~0.12, and above this ratio there is no additional uptake. The ratio of adsorbed Co : Ti$_{(surface)}$ is consistent with bidentate coordination of Co^{2+} to two Ti$_{(5c)}$–O$^-$ sites. For the present study, we prepared a series of $Co^{2+}_{(surface)}$–TiO_2 nanocrystals in which the Co : Ti mass ratio was varied from 0–0.6 (Co : Ti > 0.12 indicates a saturated surface). TEM data (Fig. 2 and S1†) indicate the morphology of the sample does not change as a result of the surface adsorption reaction, and powder X-ray diffraction data indicate the anatase TiO_2 phase is present with no other phases observed.

We hypothesized that heating the $Co^{2+}_{(surface)}$–TiO_2 nanocrystals would promote diffusion of the cobalt ions from the surface to the interior of the nanocrystal. Based on Fick's 1st law, diffusion is proportional to the concentration gradient.[38] The nanocrystals with metal ions adsorbed on the surface present a large concentration gradient to promote diffusion. We heated dispersions of $Co^{2+}_{(surface)}$–TiO_2 nanocrystals in 1-
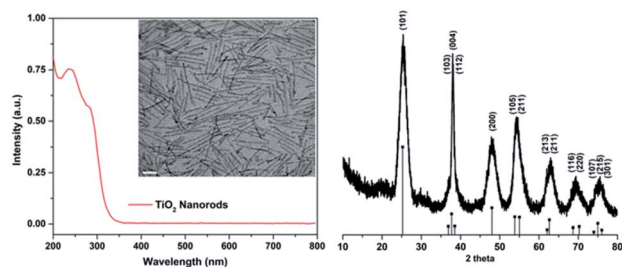

Fig. 1 Left: UV-visible absorption spectrum of TiO_2 nanorods; left (inset): transmission electron micrograph of TiO_2 nanorods (scale bar = 20 nm); right: powder X-ray diffraction pattern of TiO_2 nanorods.
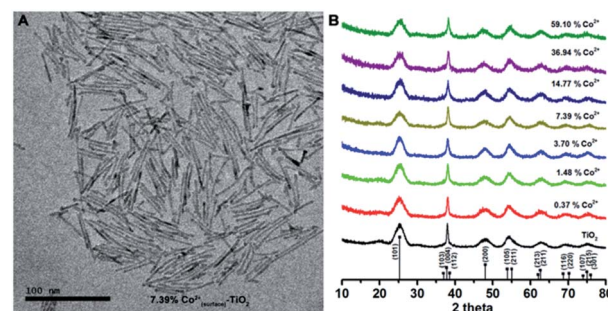

Fig. 2 (A) TEM image of $Co^{2+}_{(surface)}$–TiO_2 nanorods (Co analysis = 7.4%; others are shown in Fig. S1†); (B) powder X-ray diffraction pattern of $Co^{2+}_{(surface)}$–TiO_2 nanorods.

octadecene/trioctylphosphine oxide mixture to promote diffusion of cobalt into the nanocrystals. After the reaction was complete and brought to room temperature, addition of ethanol gave a pale blue precipitate that was isolated and redispersed in hexanes. After three cycles of precipitation/redispersion, the nanocrystals were treated with dimethylglyoxime at room temperature to remove any remaining surface cobalt ions.[23] After this step, any solution phase cobalt or surface cobalt atoms are fully removed, the color becomes light brown, and the sample contains exclusively doped cobalt in the nanocrystals. This is a key feature important in the study of $Co_{(doped)}$–TiO_2 nanocrystals. A number of reports of cobalt doping in TiO_2 nanomaterials do not include steps for removal of unbound or surface metal atoms such that the subsequent characterization and analyses may not correlate exclusively to cobalt-doped TiO_2.[39–41]

The $Co_{(doped)}$–TiO_2 nanocrystals were characterized with TEM and XRD methods (Fig. 3 and S2†). We observed rod-shape nanocrystals and powder X-ray diffraction patterns consistent with anatase TiO_2 with no other phases or morphology. The nanocrystals give stable dispersions in non-polar solvents, and TEM data indicate the samples do not aggregate. These qualitative observations indicate the feasibility of additional solution phase processing or further post-synthetic modification steps. We observe a slight contraction of the lattice parameters and unit cell volume in cobalt doped TiO_2 nanocrystals in comparison with undoped TiO_2 nanocrystals, but no apparent trend in lattice parameter as a function of dopant concentration (Fig. S3 and S4†).

Optical properties

It is noteworthy that the color of $Co^{2+}_{(surface)}$–TiO_2 is royal blue and that the product obtained after heating in 1-octadecene/trioctylphosphine oxide is light brown (Fig. 4A). Prior reports of cobalt-doped TiO_2 indicate the material has a 'light yellow' or 'tan' color.[26,42] UV-visible spectra of $Co^{2+}_{(surface)}$–TiO_2 nanocrystals (Fig. 4B) show an intense LMCT feature with two maxima at ∼240 and 286 nm, and not shifted from that found in the TiO_2 nanorods. A much weaker absorbance centered at 590 nm was assigned as spin-allowed d–d transition of the
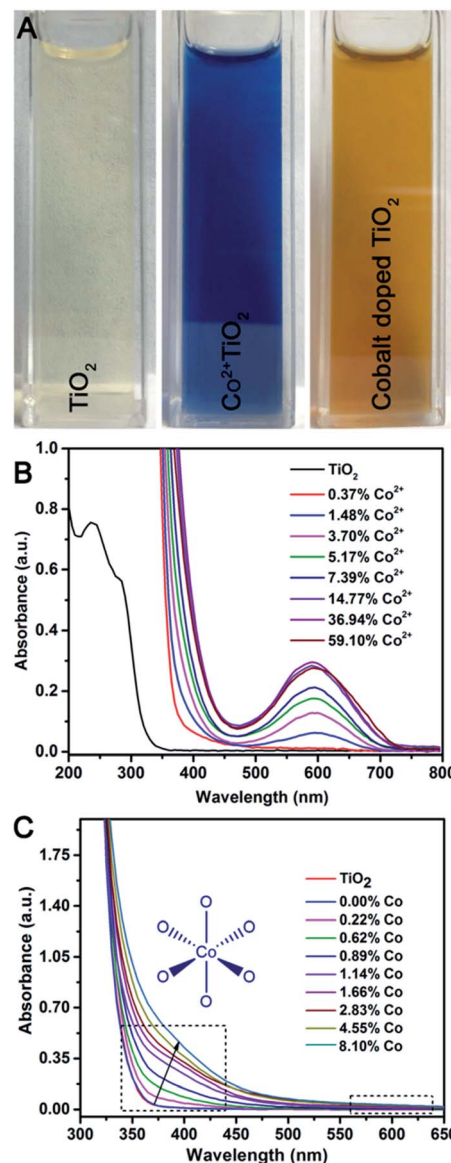

Fig. 4 (A) Photograph of (left) TiO_2 nanorods dispersed in hexanes, (middle) $Co^{2+}_{(surface)}$–TiO_2 nanorods dispersed in hexanes, and (right) $Co_{(doped)}$–TiO_2 nanorods dispersed in hexanes; (B) UV-visible absorption spectra of $Co^{2+}_{(surface)}$–TiO_2 nanocrystals; (C) UV-visible absorption spectra of $Co_{(doped)}$–TiO_2 nanocrystals.

surface Co^{2+} that gives a distinct blue color to the samples, the intensity of which varies linearly with the Co^{2+} loading on the nanocrystal surface. In contrast, the $Co_{(doped)}$–TiO_2 nanocrystals show a new absorbance feature centered ∼400 nm as a shoulder against the intense LMCT feature (Fig. 4C). The shoulder is broad and extends well into the visible region of the spectrum, which is the source of the characteristic light brown color of cobalt doped TiO_2 nanocrystals observed here and by others.[26,42] The d–d transition at 590 nm is completely absent in the $Co_{(doped)}$–TiO_2 nanocrystals.

The luminescence properties of TiO_2 nanocrystals were found to change with cobalt doping (Fig. 5). The oleic acid stabilized dispersion of TiO_2 nanorods in hexanes show a weak

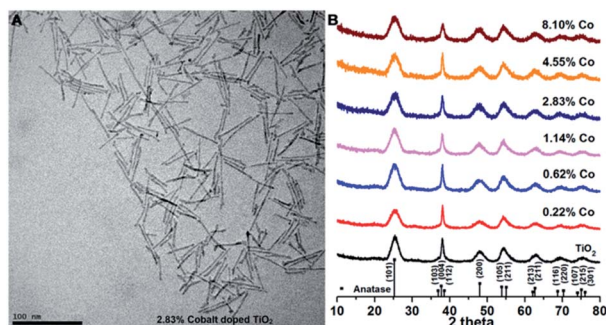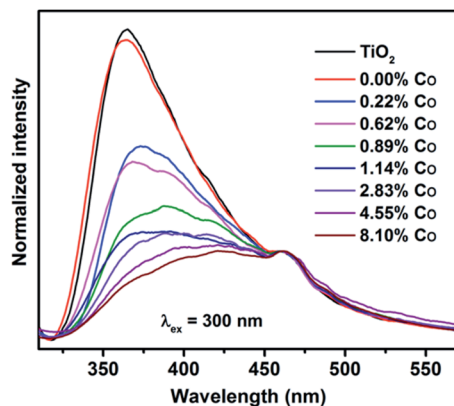Fig. 3 (A) TEM image of $Co_{(doped)}$–TiO_2 nanocrystals (cobalt analysis = 2.83%; others are shown in Fig. S2†); (B) powder X-ray diffraction pattern of $Co^{2+}_{(doped)}$–TiO_2 nanocrystals at different cobalt concentration.

Fig. 5 Emission spectra of undoped and $Co_{(doped)}$–TiO_2 nanocrystals (λ_{ex} = 300 nm). The weak feature at 460 nm is an artifact due to scattering of light from the Xe lamp; all spectra were normalized to the intensity of the artifact.
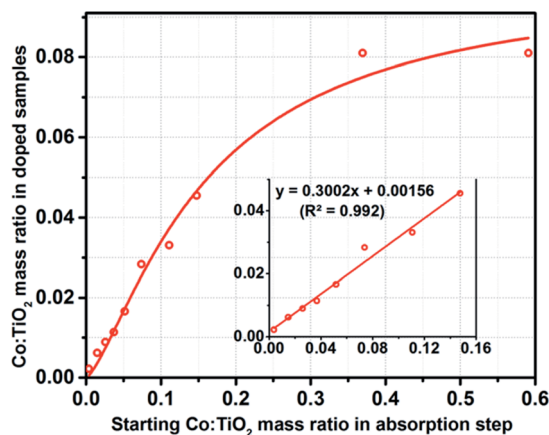

Fig. 6 Relation between Co : Ti in doped samples to Co : Ti in starting $Co_{(surface)}$–TiO_2.

emission at λ = 360 nm (λ_{ex} = 300 nm). A sample doped with 0.22% cobalt showed dramatically lowered emission with signal broadening and red-shifting. The emission from $Co_{(doped)}$–TiO_2 nanorods becomes increasingly weak, broad, and red-shifted with increasing cobalt concentration. The data suggest the doped cobalt atoms act as recombination centers with non-emissive relaxation.

An important feature of the preparation of $Co_{(doped)}$–TiO_2 nanorods was the linear correlation in the concentration of the dopant in the product to the amount of Co^{2+} adsorbed to the nanocrystal surface in the reactant. The cobalt content of the tan colored $Co_{(doped)}$–TiO_2 nanorods was measured with inductively coupled plasma atomic emission spectroscopy. A plot of Co : Ti (doped samples) *versus* Co : Ti (surface-loaded samples) yields a linear best fit (R^2 = 0.9818) with slope $\sim$0.3 (Fig. 6). The data indicate tunable doping of the nanocrystal in which $\sim$30% of the surface loaded cobalt becomes doped into the TiO_2 nanocrystal upon heating. It is important to note that the samples are free of surface bound cobalt ions and free of inorganic cobalt phases (such as Co metal, Co_3O_4, *etc.*).
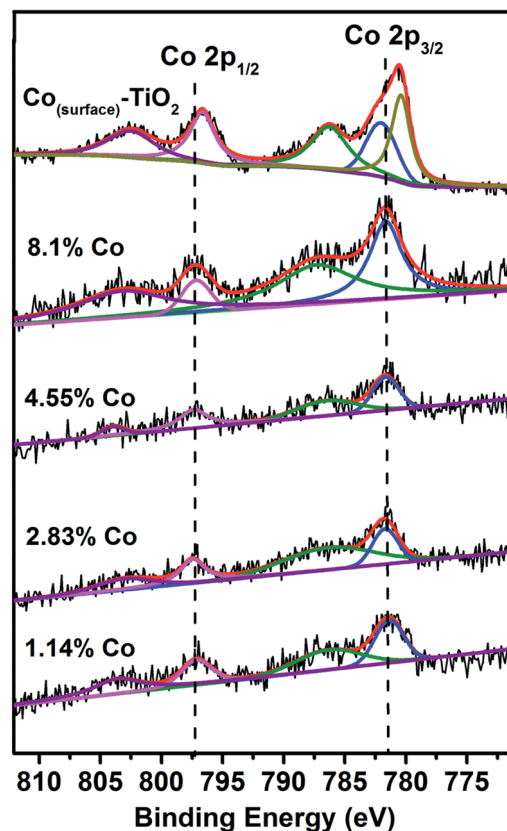

Fig. 7 XPS data from $Co_{(doped)}$–TiO_2 and $Co_{(surface)}$–TiO_2. The vertical dashed lines are set to binding energy of 781.7 eV and 797.3 eV.

X-ray photoelectron spectroscopy

XPS data of the $Co_{(doped)}$–TiO_2 nanorods were obtained. The Co 2p XPS spectra are plotted in Fig. 7. At cobalt concentration below $\sim$1%, the signal : noise was quite poor and a curve fitting analysis was not reliable; however, above this concentration the data could be modeled. We observed the Co $2p_{3/2}$ binding energy for all Co doped samples was 781.7 eV, indicating no noticeable shift in the binding energy *versus* doping concentration. We observed the Co $2p_{1/2}$ binding energy for Co doped samples was 797.3 eV, again with no appreciable shift *versus* doping concentration. The Co $2p_{3/2}$ and $2p_{1/2}$ peaks were accompanied by shake-up satellites. In comparison, the XPS spectrum of $Co_{(surface)}$–TiO_2 shows a more complex structure in the Co $2p_{3/2}$ peak with two Gaussians centered at 780.4 eV and 781.9 eV. The Co $2p_{1/2}$ peak was found at binding energy of 796.6 eV. In our previous XPS studies of $Co_{(surface)}$–TiO_2 and M,M'$_{(surface)}$–TiO_2 we observed Co $2p_{3/2}$ binding energies of 780.5–780.9 eV.[37,43] Based on the new XPS data, it is apparent that the Co $2p_{3/2}$ binding energy for $Co_{(doped)}$–TiO_2 is approximately 1 eV larger than for $Co_{(surface)}$–TiO_2. Choudhury *et al.* report binding energies of 781.4 eV and 797.2 eV for Co $2p_{3/2}$ and $2p_{1/2}$ electrons from XPS study of Co^{2+} doped TiO_2 nanoparticles.[44] Chanda *et al.* report binding energies of 781.9 eV and 797.6 eV for Co $2p_{3/2}$ and $2p_{1/2}$ electrons from XPS study of Co^{2+} doped TiO_2 nanoparticles.[45] Ali *et al.* report binding energies of 781.8 eV and 797.3 eV for Co $2p_{3/2}$ and $2p_{1/2}$ electrons

from XPS study of Co^{2+} doped TiO_2.[46] These data appear to be in fairly good agreement with our observations of Co binding energies in doped TiO_2. Tewari and Lee studied the adsorption of Co^{2+} on oxide surfaces and report Co $2p_{3/2}$ binding energy of 780.7 eV.[47] This data is in good agreement with our observations for $Co^{2+}_{(surface)}$–TiO_2.

Thin-film preparation and electrical conductivity

Thin films of $Co_{(doped)}$–TiO_2 were prepared and electrical conductivity measured. A dispersion of $Co_{(doped)}$–TiO_2 was spin-coated onto glass or ITO-coated glass substrate (ITO = indium tin oxide). The thin films were calcined at 450 °C in air for 1 h (heating rate = 9 °C min^{-1}). Film thickness could be built up with successive depositions of $Co_{(doped)}$–TiO_2. The thickness was verified from SEM images of the cross-section of the film and substrate (Fig. S5†). Each deposition step led to the formation of ∼120 nm film on the substrate. Electrical conductivity was measured with a four-point probe. The films of $Co_{(doped)}$–TiO_2 deposited on glass (no ITO layer) exhibited very high sheet resistance and measurement could not be obtained. Alternatively, a thin film of $Co_{(doped)}$–TiO_2 deposited on ITO coated glass substrate allowed direct conductivity measurement due to the shorter electrical pathway normal to the film, through the ITO layer, and back through the film to the other probe (probe separation was 1 mm). We observed the resistance increased with film thickness and that resistance decreased with increasing concentration of cobalt in the doped nano-crystal film (Fig. 8).

Magnetism

Field-dependent magnetization, M(H) curves, measured at 300 K (Fig. 9A) and 5 K (Fig. 9B) and temperature-dependent susceptibility, $\chi(T)$ curves (Fig. 9C), indicate typical paramagnetic behavior for the Co-doped TiO_2 nanocrystals.[48–50] Therefore, the $\chi(T)$ data can be expressed using the Curie–Weiss expression $\chi = \chi_0 + C/(T - \theta)$, where χ_0, C, and θ are the temperature-independent susceptibility, Curie constant, and Curie–Weiss temperature, respectively, and were obtained by
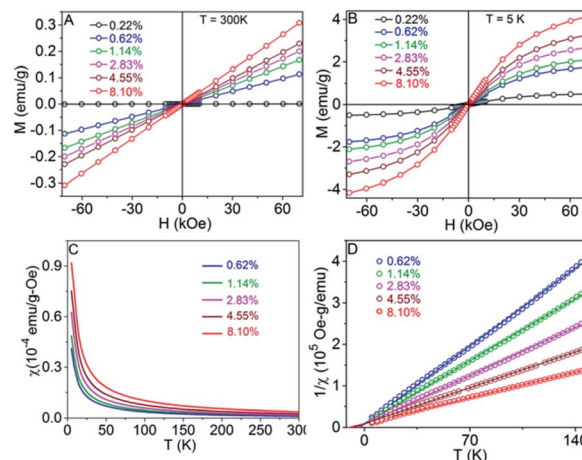

Fig. 9 Magnetic properties of Co-doped TiO_2 nanocrystals for different wt% of Co: field-dependent magnetization curves measured at 300 K (A) and 5 K (B). (C) Temperature-dependent susceptibility. (D) The inverse susceptibility is fitted using Curie–Weiss expression, where the open circles correspond to the experimental data and solid lines represent fitting results.

fitting $1/\chi$ vs. T data as shown in Fig. 9D. The effective magnetic moments per paramagnetic Co ions (μ_{eff}) in the Co-doped TiO_2 nanocrystals were determined using the C values and are in the similar range of the reported values for Co^{2+} ions.[51] The dependence of θ and μ_{eff} on Co concentration is shown in Fig. 10. The θ values are negative for all samples, which indicate antiferromagnetic interactions between Co ions. In addition, both θ and μ_{eff} decrease upon increasing the Co content, indicating an increase in antiferromagnetic coupling upon increasing Co concentration in the TiO_2 nanocrystals.

Discussion

Our observation of low-temperature antiferromagnetism in $Co_{(doped)}$–TiO_2 nanocrystal prepared from ion diffusion is in contrast to most observations of magnetic properties of cobalt
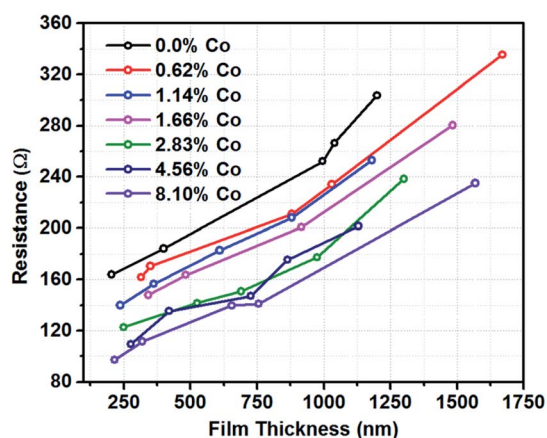

Fig. 8 Resistance versus film thickness for thin-film samples of $Co_{(doped)}$–TiO_2 on ITO-coated glass substrate.
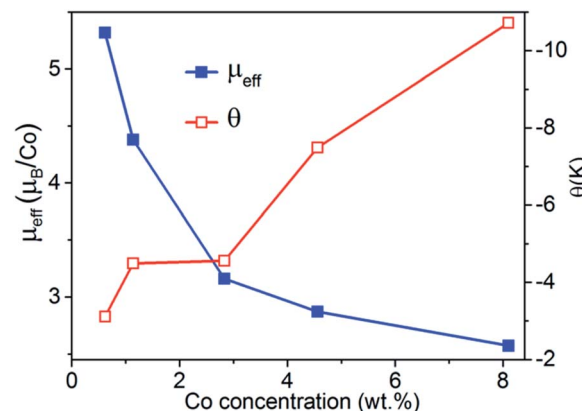

Fig. 10 Effective magnetic moment per paramagnetic Co ion and Curie–Weiss temperature as a function of Co wt% for the Co-doped TiO_2 nanocrystals.

doped TiO_2. The Koinuma group reported room-temperature ferromagnetism in cobalt-doped anatase TiO_2 thin films.[52] The Gamelin group reported paramagnetic Co^{2+}-doped TiO_2 colloidal nanocrystals, and subsequently used the colloidal nanocrystals as solution-phase precursors to prepare nanocrystalline films of Co-doped TiO_2 that displayed high-temperature ferromagnetism.[26] Room-temperature ferromagnetism in Co-doped TiO_2 materials has been reported by multiple research groups.[45,53,54] Substantial research has focused on deconvoluting the origin of magnetic properties of cobalt doped TiO_2. Depending on the synthetic method one may obtain materials with widely different magnetic properties. Under reducing conditions metallic cobalt clusters may form, which have intrinsic ferromagnetism.[55,56] In air atmosphere, metallic cobalt clusters rapidly oxidize to antiferromagnetic Co_3O_4.[44] Syntheses of cobalt doped TiO_2 at high temperature and low oxygen pressure tend to yield materials with oxygen vacancies. Several groups report oxygen vacancy dependent magnetic properties of cobalt doped TiO_2.[57–60] Janisch and Spaldin used first-principle density functional theory (DFT) calculations to study magnetism in cobalt doped TiO_2.[61] The lowest energy magnetic configuration for substitutional cobalt was ferromagnetic. Anisimov *et al.* concluded that strong interaction between cobalt and oxygen vacancies leads to three-times stronger ferromagnetism than arises from exchange interaction of cobalt ions.[62] Geng and Kim used *ab initio* DFT calculations to study magnetization arising from substitutional and interstitial cobalt sites.[63] Interstitial cobalt sites were found to be stable when paired with substitutional sites, and can either enhance or destroy magnetization of substitutional cobalt. The computational results bring considerable insight to the wide range of magnetic properties reported in cobalt doped TiO_2, especially differences arising from substitutional and interstitial dopant. However, there are few experimental data from TiO_2 solely doped with interstitial cobalt. Ogale *et al.* reported unusual antiferromagnetic behavior in a cobalt doped TiO_2 sample prepared by pulsed laser deposition in Ar/H_2 atmosphere and suggested that interstitial cobalt could play a role.[64] Yermakov *et al.* used a hydrothermal method to prepare cobalt doped TiO_2 nanopowders in which Co^{2+} was located in interstitial sites.[65] From DFT calculations, they found the most energetically favorable configuration of interstitial cobalt pairs was antiferromagnetic.

Our method for preparing $Co_{(doped)}$–TiO_2 nanocrystals is a post-synthetic modification of preformed TiO_2 nanocrystals in which the surface was loaded with Co^{2+} ions followed by cation diffusion into the nanocrystal at 250 °C. The post-synthetic approach may not favor the substitution of Ti^{4+} for Co^{2+}; whereas, a synthetic method that incorporates dopant during nanocrystal growth may be more likely to incorporate substitutional dopants. Post-synthetic substitution of Co^{2+} in Ti^{4+} sites should be strongly endergonic due to the strong electrostatic attraction between Ti^{4+} and O^{2-} ions in the TiO_2 lattice. In the cation diffusion synthesis, it may be reasonable to postulate that the Co^{2+} ions diffuse into the nanocrystal and occupy interstitial sites. In anatase TiO_2 the interstitial sites that host metals are octahedral.[66–69] We cannot go so far as to claim that

the sample consists of exclusively interstitial cobalt impurity; further characterization of the samples is required. However, our samples show room temperature paramagnetism with low temperature antiferromagnetic coupling, and the available descriptions on the origin of antiferromagnetic coupling in cobalt doped TiO_2 invoke interstitial cobalt.

Conclusions

We report the formation of $Co_{(doped)}$–TiO_2 from cation diffusion. TiO_2 nanocrystals were loaded with Co^{2+} ions on the surface followed by heating to drive the cation diffusion reaction. The product was treated with dimethylglyoxime to effectively remove surface Co^{2+} to yield exclusively $Co_{(doped)}$–TiO_2. The samples show no change in nanocrystal morphology, and no new crystalline phases in the cation surface loading or diffusion doping steps. Importantly, the concentration of the dopant could be controlled precisely based on the amount of Co^{2+} adsorbed in the initial synthesis step. Thin films of the $Co_{(doped)}$–TiO_2 show decreasing electrical resistance with increasing dopant concentration. The $Co_{(doped)}$–TiO_2 nanocrystals show room temperature paramagnetic behavior, and antiferromagnetism at low temperature. Given that the $Co_{(doped)}$–TiO_2 nanocrystals were formed under mild synthesis conditions and the unusual observation of antiferromagnetic coupling at low temperature, we preliminarily conclude that the sample contains interstitially doped cobalt.

Conflicts of interest

There are no conflicts to declare.

Acknowledgements

Notes and references

1 A. L. Efros and M. Rosen, The Electronic Structure of Semiconductor Nanocrystals, *Annu. Rev. Mater. Sci.*, 2000, **30**, 475–521.

2 M. G. Bawendi, M. L. Steigerwald and L. E. Brus, The Quantum Mechanics of Larger Semiconductor Clusters "Quantum Dots", *Annu. Rev. Phys. Chem.*, 1990, **41**, 477–496.

3 S. Link and M. A. El-Sayed, Shape and size dependence of radiative, non-radiative and photothermal properties of gold nanocrystals, *Int. Rev. Phys. Chem.*, 2000, **19**, 409–453.

4 Y. Xia, Y. Xiong, B. Lim and S. E. Skrabalak, Shape-Controlled Synthesis of Metal Nanocrystals: Simple Chemistry Meets Complex Physics?, *Angew. Chem., Int. Ed.*, 2008, **48**, 60–103.

5 Y. Jun, J. Choi and J. Cheon, Shape Control of Semiconductor and Metal Oxide Nanocrystals through Nonhydrolytic Colloidal Routes, *Angew. Chem., Int. Ed.*, 2006, **45**, 3414–3439.

6 X. Peng, Mechanisms for the Shape-Control and Shape-Evolution of Colloidal Semiconductor Nanocrystals, *Adv. Mater.*, 2003, **15**, 459–463.

7 A. R. Tao, S. Habas and P. Yang, Shape Control of Colloidal Metal Nanocrystals, *Small*, 2008, **4**, 310–325.

8 S. M. Lee, S. N. Cho and J. Cheon, Anisotropic Shape Control of Colloidal Inorganic Nanocrystals, *Adv. Mater.*, 2003, **15**, 441–444.

9 J. Owen, The coordination chemistry of nanocrystal surfaces, *Science*, 2015, **347**, 615–616.

10 M. A. Boles, D. Ling, T. Hyeon and D. V. Talapin, The surface science of nanocrystals, *Nat. Mater.*, 2016, **15**, 141–153.

11 J. D. Bryan and D. R. Gamelin, Doped semiconductor nanocrystals: synthesis, characterization, physical properties, and applications, *Prog. Inorg. Chem.*, 2005, **54**, 47–126.

12 D. J. Norris, A. L. Efros and S. C. Erwin, Doped Nanocrystals, *Science*, 2008, **319**, 1776–1779.

13 D. Mocatta, G. Cohen, J. Schattner, O. Millo, E. Rabani and U. Banin, Heavily Doped Semiconductor Nanocrystal Quantum Dots, *Science*, 2011, **332**, 77–81.

14 A. Sahu, M. S. Kang, A. Kompch, C. Nutthoff, A. W. Wills, D. Deng, M. Winterer, C. D. Frisbie and D. J. Norris, Electronic Impurity Doping in CdSe Nanocrystals, *Nano Lett.*, 2012, **12**, 2587–2594.

15 P. M. Koenraad and M. E. Flatte, Single dopants in semiconductors, *Nat. Mater.*, 2011, **10**, 91–100.

16 J. Kobak, T. Smolenski, M. Goryca, M. Papaj, K. Geitka, A. Bogucki, M. Koperski, J.-G. Rousset, J. Suffczynski, E. Janik, M. Nawrocki, A. Golnik, P. Kossacki and W. Pacuski, Designing quantum dots for solotronics, *Nat. Commun.*, 2014, **5**, 3191.

17 R. Fainblat, C. J. Barrows and D. R. Gamelin, Single Magnetic Impurities in Colloidal Quantum Dots and Magic-Size Clusters, *Chem. Mater.*, 2017, **29**, 8023–8036.

18 M. Goryca, T. Kazimierczuk, M. Nawrocki, A. Golnik, J. A. Gaj, P. Kossacki, P. Wojnar and G. Karczewski, Optical Manipulation of a Single Mn Spin in a CdTe-Based Quantum Dot, *Phys. Rev. Lett.*, 2009, **103**, 087401.

19 C. Le Gall, R. S. Kolodka, C. L. Cao, H. Boukari, H. Mariette, J. Fernández-Rossier and L. Besombes, Optical initialization, readout, and dynamics of a Mn spin in a quantum dot, *Phys. Rev. B: Condens. Matter Mater. Phys.*, 2010, **81**, 245315.

20 R. Fainblat, C. J. Barrows, E. Hopmann, S. Siebeneicher, V. A. Vlaskin, D. R. Gamelin and G. Bacher, Giant Excitonic Exchange Splittings at Zero Field in Single Colloidal CdSe Quantum Dots Doped with Individual Mn^{2+} Impurities, *Nano Lett.*, 2016, **16**, 6371–6377.

21 M. K. Nowotny, L. R. Sheppard, T. Bak and J. Nowotny, Defect Chemistry of Titanium Dioxide. Application of Defect Engineering in Processing of TiO_2-Based Photocatalysts, *J. Phys. Chem. C*, 2008, **112**, 5275–5300.

22 F. V. Mikulec, M. Kuno, M. Bennati, D. A. Hall, R. G. Griffin and M. G. Bawendi, Organometallic Synthesis and Spectroscopic Characterization of Manganese-Doped CdSe Nanocrystals, *J. Am. Chem. Soc.*, 2000, **122**, 2532–2540.

23 W. Kang, C. S. Spanjers, R. M. Rioux and J. D. Hoefelmeyer, Synthesis of brookite TiO_2 nanorods with isolated Co(II) surface sites and photocatalytic degradation of 5,8-dihydroxy-1,4-naphthoquinone dye, *J. Mater. Chem. A*, 2013, **1**, 7717–7728.

24 M. Du, S. C. Erwin and A. L. Efros, Trapped-Dopant Model of Doping in Semiconductor Nanocrystals, *Nano Lett.*, 2008, **8**, 2878–2882.

25 P. V. Radovanovic and D. R. Gamelin, Electronic Absorption Spectroscopy of Cobalt Ions in Diluted Magnetic Semiconductor Quantum Dots: Demonstration of an Isocrystalline Core/Shell Synthetic Method, *J. Am. Chem. Soc.*, 2001, **123**, 12207–12214.

26 J. D. Bryan, S. M. Heald, S. A. Chambers and D. R. Gamelin, Strong Room-Temperature Ferromagnetism in Co^{2+}-Doped TiO_2 Made from Colloidal Nanocrystals, *J. Am. Chem. Soc.*, 2004, **126**, 11640–11647.

27 R. Buonsanti and D. J. Milliron, Chemistry of Doped Colloidal Nanocrystals, *Chem. Mater.*, 2013, **25**, 1305–1317.

28 J. Zhang, Q. Di, J. Liu, B. Bai, J. Liu, M. Xu and J. Liu, Heterovalent Doping in Colloidal Semiconductor Nanocrystals: Cation-Exchange-Enabled New Accesses to Tuning Dopant Luminescence and Electronic Impurities, *J. Phys. Chem. Lett.*, 2017, **8**, 4943–4953.

29 D. Chen, R. Viswanatha, G. L. Ong, R. Xie, M. Balasubramaninan and X. Peng, Temperature Dependence of "Elementary Processes" in Doping Semiconductor Nanocrystals, *J. Am. Chem. Soc.*, 2009, **131**, 9333–9339.

30 J. Zheng, W. Ji, X. Wang, M. Ikezawa, P. Jing, X. Liu, H. Li, J. Zhao and Y. Masumoto, Improved Photoluminescence of MnS/ZnS Core/Shell Nanocrystals by Controlling Diffusion of Mn Ions into the ZnS Shell, *J. Phys. Chem. C*, 2010, **114**, 15331–15336.

31 X. Tang, W. B. A. Ho and J. M. Xue, Synthesis of Zn-Doped $AgInS_2$ Nanocrystals and Their Fluorescence Properties, *J. Phys. Chem. C*, 2012, **116**, 9769–9773.

32 V. A. Vlaskin, C. J. Barrows, C. S. Erickson and D. R. Gamelin, Nanocrystal Diffusion Doping, *J. Am. Chem. Soc.*, 2013, **135**, 14380–14389.

33 C. J. Barrows, P. Chakraborty, L. M. Kornowske and D. R. Gamelin, Tuning Equilibrium Compositions in Colloidal $Cd_{1-x}Mn_xSe$ Nanocrystals Using Diffusion Doping and Cation Exchange, *ACS Nano*, 2016, **10**, 910–918.

34 C. Balasanthiran and J. D. Hoefelmeyer, Facile method to attach transition metal ions to the surface of anatase TiO_2 nanorods, *Chem. Commun.*, 2014, **50**, 5721–5724.

35 J. Joo, S. G. Kwon, T. Yu, M. Cho, J. Lee, J. Yoon and T. Hyeon, Large-Scale Synthesis of TiO_2 Nanorods via Nonhydrolytic Sol–Gel Ester Elimination Reaction and Their Application to Photocatalytic Inactivation of *E. coli*, *J. Phys. Chem. B*, 2005, **109**, 15297–15302.

36 C. Balasanthiran, B. Zhao, C. Lin, P. S. May, M. T. Berry and J. D. Hoefelmeyer, Self-limiting adsorption of Eu^{3+} on the surface of rod-shape anatase TiO_2 nanocrystals and post-synthetic sensitization of the europium-based emission, *J. Colloid Interface Sci.*, 2015, **459**, 63–69.

37 C. Balasanthiran, S. Jensen, C. Spanjers, S. Varapragasam, R. M. Rioux, D. S. Kilin and J. D. Hoefelmeyer, Quantitative Attachment of Bimetal Combinations of Transition Metal Ions to the Surface of TiO_2 Nanorods, *Langmuir*, 2018, **34**, 5422–5434.

38 H. Mehrer, Diffusion in Solids Fundamentals, Methods, Materials, Diffusion-Controlled Processes, in *Springer Series in Solid State Sciences*, ed. M. Cardona, P. Fulde, K. von Klitzing, R. Merlin and H.-J. Quiesser, Springer-Verlag, Berlin, 2007, vol. 155.

39 K. Anbalagan, UV-Sensitized Generation of Phasepure Cobalt-Doped Anatase: $Co_xTi_{1-x}O_{2-\delta}$ Nanocrystals with Ferromagnetic Behavior Using Nano-TiO_2/*cis*-$[Co^{III}(en)_2(MeNH_2)Cl]^{2+}$, *J. Phys. Chem. C*, 2011, **115**, 3821–3832.

40 V. R. Akshay, B. Arun, G. Mandal, G. R. Mutta, A. Chanda and M. Vasundhara, Observation of Optical Band-Gap Narrowing and Enhanced Magnetic Moment in Co-Doped Sol–Gel-Derived Anatase TiO_2 Nanocrystals, *J. Phys. Chem. C*, 2018, **122**, 26592–26604.

41 Z. Zhang, Q. Wu, G. Johnson, Y. Ye, X. Li, N. Li, M. Cui, J. D. Lee, C. Liu, S. Zhao, S. Li, A. Orlov, C. B. Murray, X. Zhang, T. B. Gunnoe, D. Su and S. Zhang, Generalized Synthetic Strategy for Transition-Metal-Doped Brookite-Phase TiO_2 Nanorods, *J. Am. Chem. Soc.*, 2019, **141**, 16548–16552.

42 J. Choi, H. Park and M. R. Hoffman, Effects of Single Metal–Ion Doping on the Visible-Light Photoreactivity of TiO_2, *J. Phys. Chem. C*, 2010, **114**, 783–792.

43 A. Sathe, M. A. Peck, C. Balasanthiran, M. A. Langell, R. M. Rioux and J. D. Hoefelmeyer, X-ray photoelectron spectroscopy of transition metal ions attached to the surface of rod-shape anatase TiO_2 nanocrystals, *Inorg. Chim. Acta*, 2014, **422**, 8–13.

44 B. Choudhury, A. Choudhury, A. K. M. M. Islam, P. Alagarsamy and M. Mukherjee, Effect of oxygen vacancy and dopant concentration on the magnetic properties of high spin Co^{2+} doped TiO_2 nanoparticles, *J. Magn. Magn. Mater.*, 2011, **323**, 440–446.

45 A. Chanda, K. Rout, M. Vasundhara, S. R. Joshi and J. Singh, Structural and magnetic study of undoped and cobalt doped TiO_2 nanoparticles, *RSC Adv.*, 2018, **8**, 10939–10947.

46 B. Ali, L. R. Shah, C. Ni, J. Q. Xiao and S. I. Shah, Interplay of dopant, defects and electronic structure in driving ferromagnetism in Co-doped oxides: TiO_2, CeO_2 and ZnO, *J. Phys.: Condens. Matter*, 2009, **21**, 456005.

47 P. H. Tewari and W. Lee, Adsorption of Co(II) at the oxide–water interface, *J. Colloid Interface Sci.*, 1975, **52**, 77–88.

48 R. Pahari, B. Balasubramanian, R. Pathak, M.-C. Nguyen, S. R. Valloppilly, R. Skomski, A. Kashyap, C.-Z. Wang, K.-M. Ho, G. C. Hadjipanayis and D. J. Sellmyer, Quantum phase transition and ferromagnetism in $Co_{1+x}Sn$, *Phys. Rev. B*, 2019, **99**, 184438.

49 L. Schoop, M. Hirschberger, J. Tao, C. Felser, N. P. Ong and R. J. Cava, Paramagnetic to ferromagnetic phase transition in lightly Fe-doped Cr_2B, *Phys. Rev. B: Condens. Matter Mater. Phys.*, 2014, **89**, 224417.

50 M. M. Can, T. Firat and S. Özcan, Dominancy of antiferromagnetism in $Zn_{1-x}Co_xO$ diluted magnetic semiconductors, *J. Mater. Sci.*, 2011, **46**, 1830–1838.

51 J. S. Smart, *Effective Field Theories of Magnetism*, W.B. Saunders Company, Philadelphia, 1966.

52 Y. Matsumoto, M. Murakami, T. Shono, T. Hasegawa, T. Fukumura, M. Kawasaki, P. Ahmet, T. Chikyow, S. Koshihara and H. Koinuma, Room-Temperature Ferromagnetism in Transparent Transition Metal-Doped Titanium Dioxide, *Science*, 2001, **291**, 854–856.

53 J.-G. Li, R. Buchel, M. Isobe, T. Mori and T. Ishigaki, Cobalt-Doped TiO_2 Nanocrystallites: Radio-Frequency Thermal Plasma Processing, Phase Structure, and Magnetic Properties, *J. Phys. Chem. C*, 2009, **113**, 8009–8015.

54 C. Huang, X. Liu, Y. Liu and Y. Wang, Room temperature ferromagnetism of Co-doped TiO_2 nanotube arrays prepared by sol–gel template synthesis, *Chem. Phys. Lett.*, 2006, **432**, 468–472.

55 J.-Y. Kim, J.-H. Park, B.-G. Park, H.-J. Noh, S.-J. Oh, J. S. Yang, D.-H. Kim, S. D. Bu, T.-W. Noh, H.-J. Lin, H.-H. Hsieh and C. T. Chen, Ferromagnetism Induced by Clustered Co in Co-Doped Anatase TiO_2 Thin Films, *Phys. Rev. Lett.*, 2003, **90**, 017401.

56 A. Punnoose and M. S. Seehra, On the room temperature ferromagnetism in Co-doped TiO_2 films, *J. Appl. Phys.*, 2003, **93**, 7867–7869.

57 Y. B. Lin, Y. M. Yang, B. Zhuang, S. L. Huang, L. P. Wu, Z. G. Huang, F. M. Zhang and Y. W. Du, Ferromagnetism of Co-doped TiO_2 films prepared by plasma enhanced chemical vapour deposition (PECVD) method, *J. Phys. D: Appl. Phys.*, 2008, **41**, 195007.

58 P. Mohanty, N. C. Mishra, R. J. Choudhary, A. Banerjee, T. Shripathi, N. P. Lalla, S. Annapoorni and C. Rath, Oxygen vacancy induced phase formation and room temperature ferromagnetism in undoped and Co-doped TiO_2 thin films, *J. Phys. D: Appl. Phys.*, 2012, **45**, 325301.

59 J. H. Cho, B. Y. Kim, H. D. Kim, S. I. Woo, S. H. Moon, J. P. Kim, C. R. Cho, Y. G. Joh, E. C. Kim and D. H. Kim, Enhanced ferromagnetism in Co-doped TiO_2 powders, *Phys. Status Solidi B*, 2004, **241**, 1537–1540.

60 A. Y. Yermakov, G. S. Zakharova, M. A. Uimin, M. V. Kuznetsov, L. S. Molochnikov, S. F. Konev, A. S. Konev, A. S. Minin, V. V. Mesilov, V. R. Galakhov, A. S. Volegov, A. V. Korolyov, A. F. Gubkin, A. M. Murzakayev, A. D. Svyazhin and K. V. Melanin,

Surface Magnetism of Cobalt-Doped Anatase TiO_2 Nanopowders, *J. Phys. Chem. C*, 2016, **120**, 28857–28866.

61 R. Janisch and N. A. Spaldin, Understanding ferromagnetism in Co-doped TiO_2 anatase from first principles, *Phys. Rev. B: Condens. Matter Mater. Phys.*, 2006, **73**, 035201.

62 V. I. Anisimov, M. A. Korotin, I. A. Nekrasov, A. S. Mylnikova, A. V. Lukoyanov, J. L. Wang and Z. Zeng, The role of transition metal impurities and oxygen vacancies in the formation of ferromagnetism in Co-doped TiO_2, *J. Phys.: Condens. Matter*, 2006, **18**, 1695–1704.

63 W. T. Geng and K. S. Kim, Interplay of local structure and magnetism in Co-doped TiO_2 anatase, *Solid State Commun.*, 2004, **129**, 741–746.

64 S. Ogale, D. Kundaliya, S. Mehraeen, L. Fu, S. Zhang, A. Lussier, J. Dvorak, N. Browning, Y. Idzerda and T. Venkatesan, Chemical Inhomogeneity and Mixed-State Ferromagnetism in Diluted Magnetic Semiconductor Co : TiO_2, *Chem. Mater.*, 2008, **20**, 1344–1352.

65 A. Y. Yermakov, D. W. Boukhvalov, A. S. Volegov, M. A. Uimin, G. S. Zakharova, A. V. Korolev, E. V. Rosenfeld, V. V. Mesilov, A. S. Minin, V. R. Galakhov, L. S. Molochnikov, A. F. Gubkin, A. M. Murzakaev and S. F. Konev, Unconventional magnetism of non-uniform distribution of Co in TiO_2 nanoparticles, *J. Alloys Compd.*, 2020, **826**, 154194.

66 E. Finazzi, C. Di Valentin and G. Pacchioni, Nature of Ti Interstitials in Reduced Bulk Anatase and Rutile TiO_2, *J. Phys. Chem. C*, 2009, **113**, 3382–3385.

67 B. J. Morgan and G. W. Watson, Intrinsic n-type Defect Formation in TiO_2: A Comparison of Rutile and Anatase from GGA+U Calculations, *J. Phys. Chem. C*, 2010, **114**, 2321–2328.

68 A. Kordatos, N. Kelaidis and A. Chroneos, Migration of sodium and lithium interstitials in anatase TiO_2, *Solid State Ionics*, 2018, **315**, 40–43.

69 J. A. Dawson and J. Robertson, Improved Calculation of Li and Na Intercalation Properties in Anatase, Rutile, and TiO_2(B), *J. Phys. Chem. C*, 2016, **120**, 22910–22917.